Journal of the Optical Society of Korea
Vol. 14, No. 1, March 2010, pp. 49-54

DOI: 10.3807/JOSK.2010.14.1.049

Optical Coherence Tomography Based on a Continuous-wave Supercontinuum Seeded by Erbium-doped Fiber's Amplified Spontaneous Emission

Ju Han Lee[1], Eun Joo Jung[2,3], and Chang-Seok Kim[3]*

[1]*School of Electrical and Computer Engineering, University of Seoul, Seoul 130-743, Korea*
[2]*Nano-Photonics Research Center, Korea Photonics Technology Institute, Gwangju 500-460, Korea*
[3]*Department of Cogno Mechatronics Engineering, Pusan National University, Busan 609-735, Korea*

(Received November 16, 2009 : revised February 17, 2010 : accepted February 18, 2010)

In this study, the use of a continuous-wave (CW) supercontinuum (SC) seeded by an erbium-doped fiber's amplified spontaneous emission (ASE) for optical-coherence tomography imaging is experimentally demonstrated. It was shown, by taking an in-depth image of a human tooth sample, that due to the smooth, flat spectrum and long-term stability of the proposed CW SC, it can be readily applied to the spectral-domain optical-coherence tomography system. The relative-intensity noise level and spectral bandwidth of the CW SC are also experimentally analyzed as a function of the ASE beam power.

Keywords : Biomedical optics, Broadband light sources, Optical coherence tomography, Fiber optics, Imaging
OCIS codes : (170.3880) Medical and biological imaging; (060.2380) Fiber optic sources and detectors

I. INTRODUCTION

Optical-coherence tomography (OCT) is a highly promising method for the high-resolution, noninvasive imaging of tissue morphology in vivo [1]. Conventional OCT systems are constructed based on low-coherence interferometry, and the axial-image resolution is determined by the spectral bandwidth of the light source employed. This means that ultrabroad-bandwidth light sources must be used so that systems can obtain higher in-depth-resolution tissue images. The commonly employed broadband light sources include semiconductor-based superluminescent diodes (SLDs) [2], amplified spontaneous emission (ASE) from semiconductor optical amplifiers [3], rare-earth-doped-fiber ASE [4], and supercontinuum (SC) sources [5].

Even if good-performance OCT imaging can be achieved with the use of the light sources mentioned above, there is still a need to develop new types of light sources to improve the OCT performance. One high potential candidate is the optical-fiber-based SC source. Conventional fiber-based SC sources have been realized by using the combination of a high-peak-power subpicosecond pulse laser and a highly nonlinear optical fiber [6]. When high-peak-power pulses propagate through a highly nonlinear optical fiber, their optical spectrum is broadened due to a variety of nonlinear effects, and the spectrum is finally converted into an SC. In generating an SC from ultrashort pulses, the use of normally dispersive nonlinear fibers is essential to suppressing significant spectral modulation and amplitude fluctuations, which are caused by the nonlinear amplification of input pulse noise [7]. The pulse-mode SC has been widely investigated as a broadband source for high-resolution OCT imaging [8, 9].

On the other hand, SC was also found to be generated in the continuous-wave (CW) mode by using a partially-coherent CW pump beam [10-13]. The physical mechanism for CW SC evolution in optical fiber is slightly different from pulse-mode SC evolution [10-13]. Modulation instability (MI) converts an initial, partially-coherent CW beam coupled into a nonlinear anomalous-dispersion fiber into large numbers of ultrashort soliton-like pulses. When the noisy pulses of random peak powers and durations propagate through the fiber, stimulated Raman scattering (SRS) transforms the time-averaged spectrum of the noisy pulses into a broad and flat spectral continuum [13]. Various types of partially-coherent light sources have been proposed for the

*Corresponding author: ckim@pusan.ac.kr
Color versions of one or more of the figures in this paper are available online.

generation of CW SC; for example, a high-power Raman fiber laser [10, 14, 15], a rare-earth-doped-fiber amplified-spontaneous-emission (ASE) source [16, 17], a low-coherence-semiconductor laser diode [18], and a rare-earth-doped-fiber laser [19, 20]. It is evident that recent technological advances in implementing high-quality nonlinear optical fibers as well as high-power fiber amplifiers enable the practical implementation of stable CW SC sources. The applicability of CW SCs to OCT imaging has been investigated by Hsiung *et al*. [20]. They performed an experimental demonstration, using a CW SC source that had been generated from a high-power Yb fiber laser.

A series of investigations of CW SCs have also been carried out by our group [15, 17, 21, 22, 23]. In particular, the research has focused on CW SCs seeded by erbium-doped fiber (EDF)'s ASE in telecommunication bands because low-cost, all-fiberized optical components commonly employed for telecommunication systems can be readily used. Through our investigations, it was concluded that such applications as photonic microwave filters [22] and wavelength-division-multiplexed passive optical networks (WDM-PONs) [23], where spectrum-sliced incoherent beams are employed, could benefit from using the CW SC due to its ultrawide bandwidth and high spectral-power density.

In this study, the potential of the depolarized, incoherent CW SC in another application area (OCT imaging) is explored. More specifically, the use of an EDF's ASE-seeded CW SC for the high-performance OCT imaging of a human tooth sample is experimentally demonstrated. The implemented all-fiberized CW SC source exhibits a 3-dB spectral bandwidth of ~110 nm, covering the range from 1565~1675 nm, which corresponds to the telecommunication bands of the L-band (1565~1625 nm) and U-band (1625~1675 nm). It is known that the telecommunication band covering 1.4~1.7 μm can also be attractive for OCT imaging due to both its reduced optical scattering and its increased penetration depth at longer wavelengths [24-28]. One benefit of using telecommunication band light sources is that low-cost, all-fiberized optical components designed for telecommunication systems can be easily used. In this work, it is experimentally demonstrated that imaging of a human tooth sample can be readily achieved using a spectral-domain (SD)-OCT system incorporating the CW SC.

II. MATERIALS AND METHOD

2.1 CW Supercontinuum Seeded by Erbium-doped Fiber's ASE

The experimental setup of an SD-OCT system that incorporates the proposed ASE-based CW SC source is shown in Fig. 1. The broadband, incoherent, ASE-based CW SC was composed of a seed ASE generator based on a pumped EDF, a high-power Er/Yb amplifier, a cascade of a 1-km highly nonlinear dispersion-shifted fiber (HNL-DSF), a 10-km conventional DSF, and a 50-km standard SMF. A seed ASE beam generated from a pumped EDF was spectrum-sliced using a 3-nm bandpass filter at 1560 nm. The 3-nm ASE beam with ~-13 dBm power was amplified up to ~32 dBm using the high-power Er/Yb amplifier and was subsequently coupled into the 1-km HNL-DSF. The 10-km DSF was cascaded to the HNL-DSF. The 1-km HNL-DSF, the only available highly nonlinear optical fiber in our laboratory, is not long enough to generate sufficient nonlinear effects. The HNL-DSF and DSF, both of which had a zero dispersion wavelength (λ_0) of 1550 nm exhibited nonlinearity parameters (γ) of ~28 and ~2 $W^{-1} \cdot km^{-1}$, respectively, and their narrowband ASE beam was converted into a depolarized spectral continuum due to the combined effects of MI and SRS [13, 14]. MI leads to soliton-like structure formation that experiences subsequent self-Raman interaction. The Raman soliton formation is induced by the random phase and intensity fluctuations of the pump beam propagating through an anomalous-dispersion optical fiber. The large numbers of noisy solitonic structures randomly distributed in space and time give rise to a broad spectral continuum. The 50-km SMF was used as a broadband attenuator to reduce the SC power output to ~15 dBm as a broadband inline attenuator covering the L- and U-bands was not available in our laboratory. Further details on the CW SC source are provided in Ref. [17].

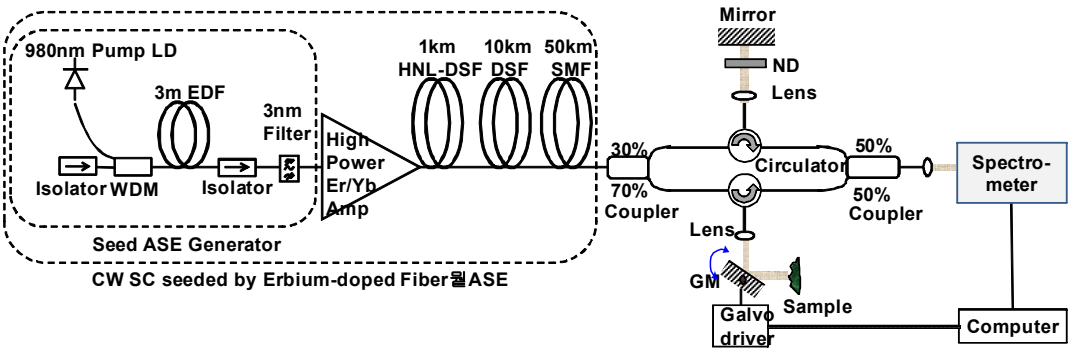

FIG. 1. Experimental schematic diagram of the proposed OCT imaging system incorporating a CW SC seeded by EDF's ASE. Abbreviations: ND, neutral-density filter; GM, galvanometer mirror.

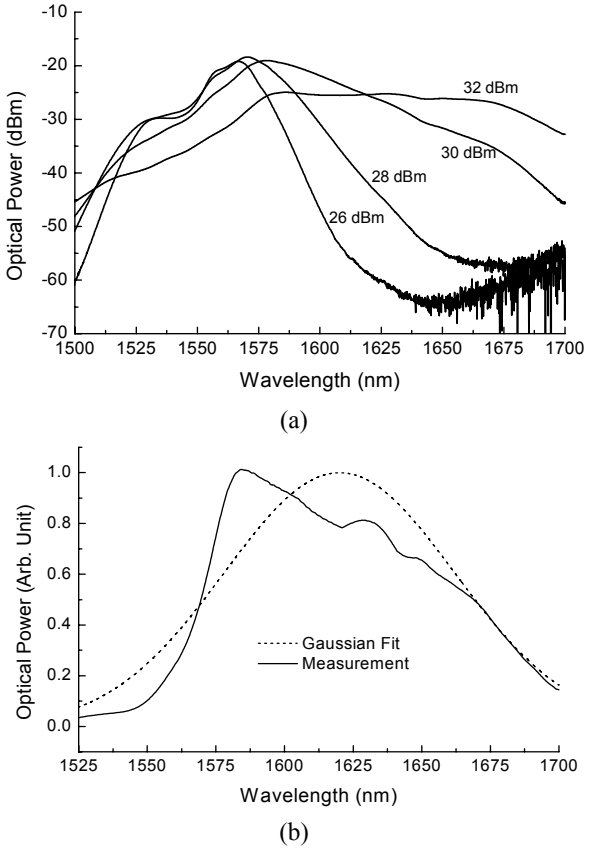

FIG. 2. (a) Measured optical spectra of the CW SC for various power levels of the amplified 3-nm-bandwidth ASE beam. (b) A linear scaled view of the optical spectrum of the CW SC at an amplified 3-nm-bandwidth ASE beam power of 32 dBm.

Fig. 2(a) shows the output spectra measured as a function of the amplified 3-nm-bandwidth ASE beam that was coupled into the HNL-DSF. The output spectrum from the 50-km SMF was observed to broaden and flatten as the amplified 3-nm-bandwidth ASE beam power was increased. A linear scaled view of the output SC spectrum at an amplified 3-nm-bandwidth ASE beam power of 32 dBm is shown in Fig. 2(b). As a matter of fact, the sharp spectral edge, which was observed at short wavelengths, is undesirable as it causes side lobes in the axial point spread function (PSF). At present, attempts are being made to improve the SC spectral shape without using external spectral-shaping filters as external spectral shaping may result in the decrease of the spectral bandwidth. The full-width half-maximum of the SC bandwidth was determined to be ~110 nm, centered at ~1595 nm, and the corresponding theoretical axial resolution (Δz) of imaging was estimated to be 10.2 μm using the following simple relation [1]:

$$\Delta z = \frac{2\ln(2)\lambda^2}{\pi\Delta\lambda} \tag{1}$$

where λ and $\Delta\lambda$ are the center wavelength and the spectral bandwidth of the broadband source, respectively.

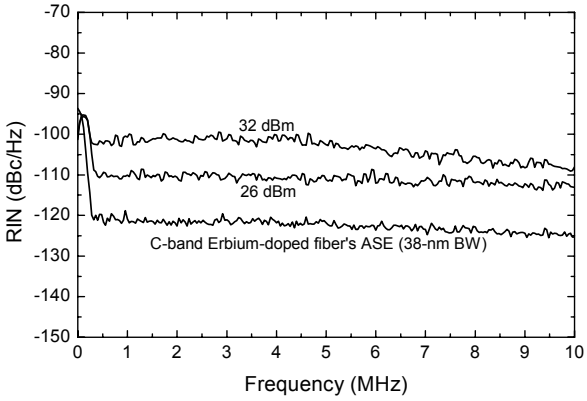

FIG. 3. Measured relative-intensity noise levels of the EDF's ASE-seeded CW SC for various power levels of the amplified 3-nm-bandwidth ASE beam together with that of C-band EDF's ASE.

One concern in investigating the applicability of CW SC to OCT imaging is its relative-intensity-noise (RIN) level because RIN can affect the sensitivity and dynamic range [29]. First, RIN measurement of the SC output was performed as a function of the amplified 3-nm-bandwidth ASE beam power by launching the SC output onto a low-noise photodetector with a bandwidth of 10 MHz, which was AC-coupled into an electrical spectrum analyzer. The measured RIN spectra are shown in Fig. 3 together with that of the full C-band EDF's ASE. As we were interested in RIN within the typical demodulation range of OCT systems, the RIN measurement was carried out within the range of 0.01~10 MHz. The RIN level of the CW SC was found to be much higher than that of EDF's ASE even if the CW SC was seeded by EDF's ASE. Specifically, the CW SC RIN level at an amplified 3-nm-bandwidth ASE beam power of 32 dBm was found to be ~20 dB larger than that of the full C-band ASE. Furthermore, contrary to the well-known fact that the RIN of an incoherent broad-bandwidth light source is inversely proportional to its spectral bandwidth [30], the RIN of the CW SC was found to increase with the spectral bandwidth, as shown in Fig. 4. Such a high RIN level is believed to be due to stimulated-Raman-process-induced, amplified pump-to-stokes RIN transfer [31]. Note that the CW SC is generated mainly by the combination of the MI and SRS processes. The high RIN level of the CW SC might degrade the OCT imaging performance. The impact of RIN on the imaging quality can be indirectly inferred from the estimation of signal-to-noise ratio (SNR) of the light source. Note that the SNR estimation is commonly used for the evaluation of signal quality in telecommunication systems. The SNR limitation caused by RIN can be expressed as [32]

$$SNR = \Big/ \int_{f_0}^{f_1} RIN(f)\,df \tag{2}$$

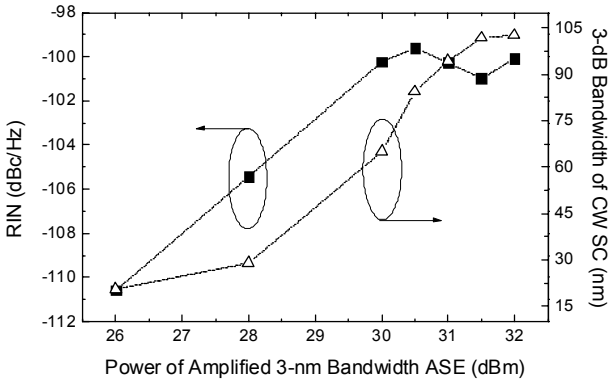

FIG. 4. RIN level and spectral bandwidth of the EDF's ASE-seeded CW SC as a function of the amplified 3-nm-bandwidth ASE beam power.

where f_0 and f_1 are the electrical frequencies. Assuming that the typical demodulation frequency range of OCT systems is 0 ~ 10 MHz, f_0 and f_1 become 0 and 10 MHz, respectively. Using eq. (2) the SNR for the CW SC was estimated to be ~32 dB, which is ~ 12 dB lower than that of the full C-band EDF's ASE (~ 44 dB). Even if the CW SC source exhibits a relatively low SNR compared to the full C-band EDF's ASE, the SNR value of ~32 dB is believed to cause no significant degradation of imaging quality. This fact needs to be confirmed by a further investigation. Note that in fiber optic communication systems a transmitted, incoherent signal with a SNR more than 18 dB can be detected at the receiver end without bit errors (Bit Error Rate < 10^{-14}) [30].

2.2 Experimental OCT Setup Incorporating the CW Supercontinuum

Bearing in mind that the high RIN level of the CW SC may significantly affect the OCT imaging performance, we executed an exemplary demonstration of the use of the developed CW SC. As shown in Fig. 1, the OCT imaging setup was based on a Mach-Zehnder interferometer. A cross-sectional image was produced by transversely scanning the beam across a sample using a galvanometer (GM), and by collecting a reflected profile at each point. The reflected intensities were recorded on a grayscale image as a function of the transverse and axial distances. An optical spectrum analyzer (OSA: AQ6317B, produced by ANDO Electronic Co.) was used in place of a spectrometer to obtain most of the OCT experimental data in this experiment, because an InGaAs-type CCD spectrometer for a 1550-nm region was not available in our laboratory [2]. The acquired data from the OSA was transferred to a computer through a shielded general-purpose interface bus cable (GPIB, produced by National Instruments) [33]. The maximum GPIB transfer rate was more than 7.2 Mb/s. The acquired data was processed and visualized using the customized software written with LabView®.

2.3 Human Tooth Sample

A human tooth sample was carefully prepared for the experimental demonstration. As enamel and dentin possess ~2 and ~18% water concentrations, which are substantially lower than that of the skin, their dominant light loss factor is scattering rather than water absorption. Furthermore, the fact that smaller scattering exists at the 1500~1700 nm bands than at the 800 or 1300 nm band allows for low-noise imaging. Note that scattering decreases at longer wavelengths in proportion to $(1/\lambda^4)$, indicating that the magnitude at the 1500~1700 nm wavelengths is over 30 times lower than that at the visible wavelengths [28].

III. RESULTS AND DISCUSSION

The shorter the coherence length of the source, the more closely the sample and reference arm group delays must be matched for constructive interference to occur. The OCT system performance was characterized by measuring the PSF using a mirror as a sample. At the 1.2-mm imaging axial distance measured in air, the experimentally determined axial resolution was ~12.2 μm whereas the theoretical resolution with the Gaussian spectrum was ~10.2 μm for the output CW SC spectrum at an amplified 3-nm-bandwidth ASE beam power of 32 dBm. The degradation of the axial resolution can be attributed to various factors, such as the non-Gaussian spectral shape of the light source, the use of a Hamming spectral window before discrete Fourier transform (DFT), and the wavelength dependence of the fiber-optic components employed. To analyze the changes in the dynamic range from the SC source, the point spread functions (PSFs) for variable lengths of the reference arm were measured as presented in Fig. 5(a). Since the proposed OCT system using an OSA showed a larger optical-saturation power limit, it was not easy to define the overall sensitivity value of this SD-OCT system. The maximum dynamic range of the logarithm-scaled PSFs at the optical length of 110 μm was found to be ~40 dB, which was determined by detecting the minimum visible intensity of a mirror reflection at the position of the sample with the incident source power of 30 mW.

Fig. 5(b) shows the obtained OCT image of the sample human tooth sample. The image had 256 transverse pixels and 512 axial pixels. Due to the data acquisition mechanism that was used, the quality of the OCT image acquired using an OSA could not be as high as that acquired using a conventional CCD spectrometer, as explained in Ref. [2]. It is expected that a higher-quality OCT image can be obtained with the proposed light source only if an InGaAs-type CCD spectrometer for a 1550-nm region is employed in the proposed OCT imaging system. The required time for acquiring the interference signal of an A-line using the OSA over a 130 nm bandwidth in a high-sensitivity-mode resolution bandwidth of 0.05 nm is more than 1.3 s. One of the critical factors contributing to the production of

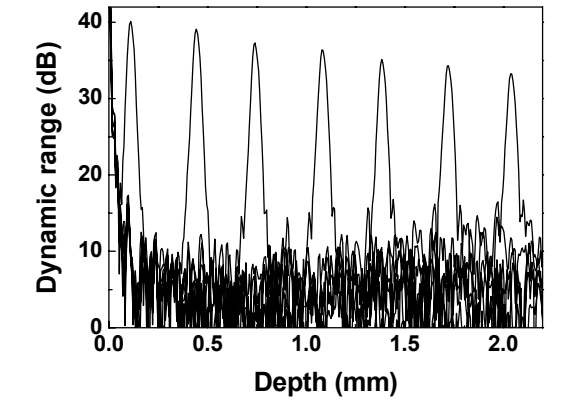

(a)

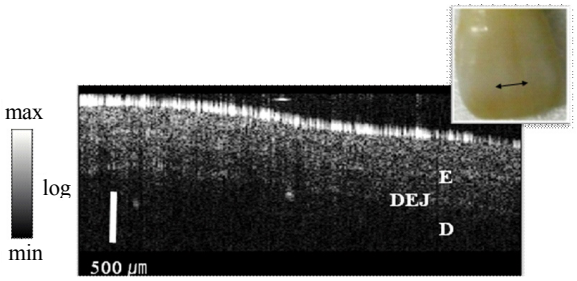

(b)

FIG. 5. (a) Measured axial point spread functions at various optical-length differences. (b) OCT image of a human tooth sample. The brighter regions correspond to the areas with a larger backscattered intensity (unit: dB). A picture of the sample surface is shown in the inset. The double-headed arrow indicates the sample's scan range for the OCT image. Abbreviations: E, enamel; D, dentin; DEJ, dentoepithelial junction.

significant signal distortion in the SD-OCT system is the fringe washout phenomenon, which is caused by a very slow readout process. This means that an OCT system using an OSA cannot produce an image with quality as high as that of the images acquired using a conventional CCD spectrometer. Variability in enamel morphology was still evident, however, with a sharp drop in the coherent backscattered intensity clearly delineating the junction between the enamel and dentin layers, as shown in Fig. 5(b). The inset shows a surface picture of the human tooth sample. The double-headed arrow in the inset indicates the scan range of the light source which traverses the direction for the OCT image.

IV. CONCLUSION

The possibility of using a depolarized, incoherent CW SC seeded by EDF's ASE as a broadband source for SD-OCT imaging was investigated. Such a CW SC showed a smooth and flat spectrum as well as long-term stability. It was experimentally shown that the CW SC could be readily applied to the OCT imaging of a human tooth sample. As a matter of fact, several high-quality works on the OCT imaging of human teeth have already been carried out with ~800- and ~1300-nm light sources [34-37]. Even if the image quality obtained with the CW SC in this work is not superior to that obtained in the previous demonstrations using conventional light sources, it can be concluded from our feasibility demonstration that higher-quality OCT images can be achieved through the further optimization and improvement of the OCT setup using a CCD spectrometer, or through the Gaussian spectral shaping of the output CW SC beam.

V. ACKNOWLEDGEMENT

This research was supported by Basic Science Research Program through the National Research Foundation of Korea (NRF) funded by the Ministry of Education, Science and Technology (R01-2007-000-20553-0).

REFERENCES

1. D. Huang, E. A. Swanson, C. P. Lin, J. S. Schuman, W. G. Stinson, W. Chang, M. R. Hee, T. Flotte, K. Gregory, C. A. Puliafito, and J. G. Fujimoto, "Optical coherence tomography," Science **254**, 1178-1181 (1991).
2. E. J. Jung, J. S. Park, M. Y. Jeong, C. S. Kim, T. J. Eom, B. A. Yu, S. Gee, J. Lee, and M. K. Kim, "Spectrally-sampled OCT for sensitivity improvement from limited optical power," Opt. Exp. **16**, 17457-17467 (2008).
3. J. H. Kim and B. H. Lee, "Murine heart wall imaging with optical coherence tomography," J. Opt. Soc. Korea **10**, 42-47 (2006).
4. B. E. Bouma, L. E. Nelson, G. J. Tearney, D. J. Jones, M. E. Brezinski, and J. G. Fujimoto, "Optical coherence tomographic imaging of human tissue at 1.55 μm and 1.81 μm using Er and Tm-doped fiber sources," J. Biomed. Opt. **3**, 76-79 (1998).
5. N. Nishizawa, Y. Chen, P. Hsiung, E. P. Ippen, and J. G. Fujimoto, "Real-time, ultrahigh-resolution, optical coherence tomography with an all-fiber, femtosecond fiber laser continuum at 1.5 μm," Opt. Lett. **29**, 2846-2848 (2004).
6. P. S. Westbrook, J. W. Nicholson, K. S. Feder, and A. D. Yablon, "Improved supercontinuum generation through UV processing of highly nonlinear fibers," IEEE J. Lightwave Technol. **23**, 13-18 (2005).
7. K. L. Corwin, N. R. Newbury, J. M. Dudley, S. Coen, S. A. Diddams, K. Weber, and R. S. Windeler, "Fundamental noise limitations to supercontinuum generation in microstructure fiber," Phys. Rev. Lett. **90**, 113904 (2003).
8. S. Bourquin, A. D. Aguirre, I. Hartl, P. Hsiung, T. H. Ko, J. G. Fujimoto, T. A. Birks, W. Wadsworth, U. Bunting, and D. Kopf, "Ultrahigh resolution real time OCT imaging using a compat femtosecond Nd:Glass laser and nonlinear fiber," Opt. Exp. **11**, 3290-3297 (2003).
9. Y. Wang, I. Tomov, J. S. Nelson, Z. Chen, H. Lim, and F. Wise, "Low-noise broadband light generation from optical fibers for use in high-resolution optical coherence tomo-

graphy," J. Opt. Soc. Am. A **22**, 1492-1499 (2005).
10. S. Martin-Lopez, M. Gonzalez-Herraez, A. Carrasco-Sanz, F. Vanholsbeeck, S. Coen, H. Fernandez, J. Solis, P. Corredera, and M. L. Hernanz, "Broadband spectrally flat and high power density light source for fiber sensing purposes," Meas. Sci. Technol. **17**, 1014-1019 (2006).
11. M. Prabhu, N. S. Kim, and K. Ueda, "Ultra-broadband CW supercontinuum generation centered at 1483.4 nm from Brillouin/Raman fiber laser," Jpn. J. Appl. Phys. **39**, L291-L293 (2000).
12. A. V. Avdokhin, S. V. Popov, and J. R. Taylor, "Continuous-wave, high-power, Raman continuum generation in holey fibers," Opt. Lett. **28**, 1353-1355 (2003).
13. S. M. Kobtsev and S. V. Smirnov, "Modelling of high-power supercontinuum generation in highly nonlinear, dispersion shifted fibers at CW pump," Opt. Exp. **13**, 6912-6918 (2005).
14. A. K. Abeeluck, C. Headley, and C. G. Jørgensen, "High-power supercontinuum generation in highly nonlinear dispersion-shifted fibers by use of a continuous-wave Raman fiber laser," Opt. Lett. **29**, 2163-2165 (2004).
15. J. H. Lee, Y. Takushima, and K. Kikuchi, "Continuous-wave supercontinuum laser based on an erbium-doped fiber ring cavity incorporating a highly nonlinear fiber," Opt. Lett. **30**, 2599-2602 (2005).
16. C. J. S. de Matos, S. V. Popov, and J. R. Taylor, "Temporal and noise characteristics of continuous-wave pumped continumm generation in holey fibers around 1300 nm," Appl. Phys. Lett. **85**, 2706-2708 (2004).
17. J. H. Lee, Y.-G. Han, and S. B. Lee, "Experimental study on seed light source coherence dependence of continuous-wave supercontinuum performance," Opt. Exp. **14**, 3443-3452 (2006).
18. A. K. Abeeluck and C. Headley, "Supercontiuum growth in a highly nonlinear fiber with a low-coherence semiconductor laser diode," Appl. Phys. Lett. **85**, 4863-4865 (2004).
19. P. A. Champert, V. Couderc, and A. Barthelemy, "1.5-2.0 μm multiwatt continuum generation in dispersion-shifted fiber by use of high-power continuous-wave fiber source," IEEE Photon. Technol. Lett. **16**, 2445-2447 (2004).
20. P. L. Hsiung, Y. Chen, T. H. Ko, J. G. Fujimoto, C. J. S. de Matos, S. V. Popov, J. R. Taylor, and V. P. Gapontsev, "Optical coherence tomography using a continuous-wave, high-power, Raman continuum light source," Opt. Exp. **12**, 5287-5295 (2004).
21. C. S. Kim and J. U. Kang, "Multi-wavelength switching of Raman fiber ring laser incorporating composite PMF Lyot-Sagnac filter," Appl. Opt. **43**, 3151-3157 (2004).
22. J. H. Lee, Y.-M. Chang, Y.-G. Han, S. B. Lee, and H. Chung, "Fully reconfigurable photonic microwave transversal filter based on digital micromirror device and continuous wave, incoherent supercontinuum source," Appl. Opt. **46**, 5158-5167 (2007).
23. J. H. Lee, K. Lee, Y.-G. Han, S. B. Lee, and C. H. Kim, "Single, depolarized, CW supercontinuum-based wavelength division multiplexed passive optical network architecture with C-band OLT, L-band ONU, and U-band monitoring," IEEE J. Lightwave Technol. **26**, 2891-2897 (2007).
24. N. Nishizawa, Y. Chen, P. Hsiung, E. P. Ippen, and J. G. Fujimoto, "Real-time, ultrahigh-resolution, optical coherence tomography with an all-fiber, femtosecond fiber laser continuum at 1.5 μm," Opt. Lett. **29**, 2846-2848 (2004).
25. D. Choi, T. Amano, H. Hiro-Oka, H. Furukawa, T. Miyazawa, R. Yoshimura, M. Nakanishi, K. Shimizu, and K. Ohbayashi, "Tissue imaging by OFDR-OCT using an SSG-DBR laser," Proc. SPIE **5690**, 101-113 (2005).
26. A. Unterhuber, B. Povazay, K. Bizheva, B. Hermann, H. Sattmann, A. Stingl, T. Le, M. Seefeld, R. Menzel, M. Preusser, H. Budka, C. Schubert, H. Reitsamer, P. K. Ahnelt, J. E. Morgan, A. Cowey, and W. Drexler, "Advances in broad bandwidth light sources for ultrahigh resolution optical coherence tomography," Phys. Med. Biol. **49**, 1235 (2004).
27. U. Sharma, E. W. Chang, and S. H. Yun, "Long wavelength optical coherence tomography at 1.7 μm for enhanced imaging depth," Opt. Exp. **16**, 19712-19723 (2008).
28. D. Fried, R. E. Glena, J. D. B. Featherstone, and W. Seka, "Nature of light scattering in dental enamel and dentin at visible and near-infrared wavelengths," Appl. Opt. **34**, 1278-1285 (1995).
29. S. Moon and D. Y. Kim, "Normalization detection scheme for high-speed optical frequency-domain imaging and reflectometry," Opt. Exp. **15**, 15129-15146 (2007).
30. J. S. Lee, C. H. Chung, and D. J. Digiovanni, "Spectrum-sliced fiber amplifier light source for multi-channel WDM application," IEEE. Photon. Technol. Lett. **5**, 1458-1461 (1998).
31. C. R. S. Fludger, V. Handerek, and R. J. Mears, "Pump to signal RIN transfer in Raman fiber amplifiers," IEEE J. Lightwave Technol. **19**, 1140-1148 (2001).
32. K. Sato and H. Toba, "Reduction of mode partition noise by using semiconductor optical amplifiers," IEEE J. Select. Topics Quantum Electron. **7**, 328-333 (2001).
33. H. S. Lee, E. J. Jung, M. Y. Jeong, and C. S. Kim, "Broadband wavelength-swept Raman laser for Fourier-domain mode locked swept-source OCT," J. Opt. Soc. Korea **13**, 316-320 (2009).
34. D. D. D. Fonseca, B. B. C. Kyoyoku, A. M. A. Maia, and A. S. L. Gomes, "*In vitro* imaging of remaining dentin and pulp chamber by optical coherence tomography: comparison between 850 and 1280 nm," J. Biomed. Opt. **14**, 024009-1~024009-5 (2009).
35. V. D. Madjarova, Y. Yasuno, S. Makita, Y. Hori, M. Yamanari, M. Itoh, T. Yatagai, M. Tamura, and T. Nanbu, "In-vivo three dimensional Fourier-domain optical coherence tomography for soft and hard oral tissue measurements," in *Proc. Biomedical Optics Topical Meeting (BIOMED)* (Fort Lauderdale, FL, USA, Mar. 2006), paper WE3.
36. F. I. Feldchtein, G. V. Gelikonov, V. M. Gelikonov, R. R. Iksanov, R. V. Kuranov, A. M. Sergeev, N. D. Gladkova, M. N. Ourutina, J. A. Warren, and D. H. Reitze, "In vivo OCT imaging of hard and soft tissue of the oral cavity," Opt. Exp. **3**, 239-250 (1998).
37. S. S. Manesh, C. L. Darling, and D. Fried, "Polarization-sensitive optical coherence tomography for the nondestructive assessment of the remineralization of dentin," J. Biomed. Opt. **14**, 044002-1~044002-6 (2009).